Schottky-to-Ohmic Crossover in Carbon Nanotube Transistor Contacts

V. Perebeinos, J. Tersoff,* and W. Haensch
IBM T.J. Watson Research Center, Yorktown Heights, New York 10598, USA
(Received 12 August 2013; published 4 December 2013)

For carbon nanotube transistors, as for graphene, the electrical contacts are a key factor limiting device performance. We calculate the device characteristics as a function of nanotube diameter and metal work function. Although the on-state current varies continuously, the transfer characteristics reveal a relatively abrupt crossover from Schottky to Ohmic contacts. We find that typical high-performance devices fall surprisingly close to the crossover. Therefore, tunneling plays an important role even in this regime, so that current fails to saturate with gate voltage as was expected due to ''source exhaustion.''

DOI: 10.1103/PhysRevLett.111.236802 PACS numbers: 73.63.Fg, 73.40.Cg, 73.63.Rt

Since the earliest studies of carbon nanotube field-effect transistors (CNT FETs), the metal contacts have been a key factor limiting device performance. Many of the issues that first arose with CNT FETs are also crucial for devices based on graphene or dichalcogenides. For CNTs, early contacts were invariably dominated by Schottky barriers [1–3]. A major breakthrough came with the fabrication of robust low-resistance contacts [4], although so far only for p-type contacts. Correspondingly, models of CNT contacts generally focus on one of two simple regimes. For Schottky contacts, the focus is exclusively on transmission through the barrier, with the gate serving to thin the barrier and increase tunneling. For Ohmic contacts, incidental local barriers can still play some role, but for many purposes these can be neglected, especially for thin gate oxides [5]. Then for ballistic devices, the on-state current $I_{\rm on}$ is expected to be limited by ''source exhaustion'': the maximum possible current is set by the contact doping (i.e., the carrier density provided by charge transfer from the metal) times its average velocity [6–8].

This simple dichotomy has proven adequate for general discussions, but it has never been directly confirmed by experimental measurements. Even in nominally Ohmic CNT FETs it is difficult to distinguish source exhaustion from other effects that could cause $I_{\rm on}$ to saturate with increasing gate voltage. More importantly, the height of any Schottky barrier is expected to vary in a simple way with metal work function and CNT band gap. Therefore, one might expect a strong dependence of $I_{\rm on}$ on these factors, up to the point at which the barrier vanishes, and a much weaker dependence in the Ohmic regime. However, the only experiment to directly address this reported a strikingly continuous dependence spanning the entire range from good devices to high-resistance contacts [9].

Here we calculate the behavior of CNT FETs using a device model that is applicable across both regimes. Consistent with Ref. [9], we find that when one simply examines on-state current $I_{\rm on}$ there is no clear transition between regimes, only a smooth variation with metal work function and CNT band gap. However, a clear transition is present in other performance metrics, with a qualitative change in the shape of the transfer characteristics. Comparison with experiment indicates that typical high-performance devices operate in a regime surprisingly close to the Schottky-Ohmic crossover. This suggests the possibility of further improvements in device performance via work function engineering.

We find that device characteristics in the Ohmic regime are rather different than expected. In particular, simple source exhaustion is not observed in our calculations. This is fortunate, because current saturation with gate voltage is undesirable for transistors. Instead, the current continues to rise with increasing gate voltage. The reason is that, while the doping in the CNT is limited, there are plenty of carriers in the metal at energies within the CNT band gap. These metal states can tunnel to the channel via evanescent states in the CNT underneath the metal contact. This tunneling increases continuously with gate voltage, and is particularly large for the thin gate oxides used in advanced high-performance devices.

Our computational method is an extension of semiclassical device modeling to include tunneling, as well as electronic coupling between the CNT and the metal in the usual side-contact configuration. All energies are measured relative to ground, i.e., to the source Fermi level. For energies outside the band gap, the distribution function $f_i^r(x, E)$ for a right-moving carrier resolved by energy E and band index i obeys

$$0 = -\frac{df_i^r(E,x)}{dx} + \frac{f_i^r(E,x) - f^0[E - E_F^M(x)]}{v_i(E,x)\tau_M(E,x)} + \frac{f_i^r(E,x) - f^0[E - E_{\rm loc}(x)]}{v_i(E,x)\tau_{\rm scat}(E,x)}, \quad (1)$$

where $v_i(E,x)$ is the band velocity, the τ's are relaxation times, and f^0 is the Fermi-Dirac distribution. The second term describes an electrical coupling to the metal [10], which provides a source of current into and out of the nanotube [11]. For left-moving carriers, the sign of $v_i(E,x)$ in Eq. (1) is reversed. The third term allows

thermalization of the carriers toward an equilibrium distribution within a relaxation-time approximation, with the local quasi-Fermi level $E_{\rm loc}(x)$ found self-consistently [12]. Further details of the model are given in Ref. [13]. We can express current density $j_i(E,x)$ resolved by energy and band index, and total current I, as

$$j_i(E,x) = \frac{4e}{h}[f_i^r(E,x) - f_i^l(E,x)]$$
$$I(x) = \sum_i \int_{-\infty}^{\infty} j_i(E,x)dE. \quad (2)$$

At a given energy, if two regions of propagating states (including metal states) are separated by a region with no states at that energy, we use the tunneling probability to set boundary conditions for transmission and reflection at the classical turning point. (Inelastic tunneling is not considered.) Carrier transfer at each point along the metal-CNT side contact is treated assuming an energy-independent transfer rate. In this way, we can consistently describe both ballistic and diffusive transport, with Schottky or Ohmic contacts, including ambipolar devices.

We focus on nearly ballistic devices in the ideal cylindrical geometry, in which both the contact and gate wrap around the CNT, as shown in Fig. 1. This figure also illustrates schematically the current pathway from the channel to the metal. In a Schottky contact, the source Fermi level falls in the CNT band gap, so the states in CNT region I are evanescent (regardless of V_g), but they still provide a path for tunneling between the metal and the channel.

The carrier distribution function $f^{r(l)}(E,x)$ is calculated self-consistently, with the metal gate and contacts providing electrostatic boundary conditions. The CNT multiband electronic structure is described by a one-parameter (pi-only) tight-binding model. Device parameters are chosen to facilitate comparison with experiment [9]; see Ref. [14] for specific values. Following Ref. [9] we define the on-state current $I_{\rm on}$ by overdrive $V_g - V_t = -0.5$ V.

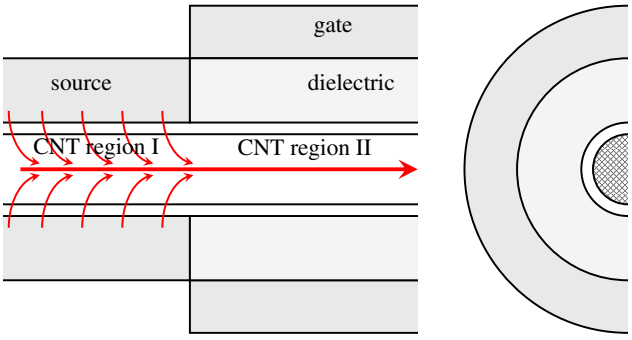

FIG. 1 (color online). Gate-all-around device geometry used here. On the left is the cross section of contact region, on the right is a view down the axis. The red arrows schematically illustrate the current paths from metal to the channel.

The drain voltage $V_d = -0.5$ V, which is usually enough to saturate current in the regime of greatest interest.

Figure 2 shows $I_{\rm on}$ as a function of CNT diameter, for metals with a range of work functions. The qualitative trends are well understood from simple band-alignment arguments. Relative to the vacuum level, the metal Fermi level is at $-W_m$ and the CNT valence edge is at $-W_c - E_g/2$, where W_m and W_c are the work functions of the metal and a metallic CNT, respectively, and E_g is the CNT band gap, which scales with diameter as $E_g \propto 1/d$. Thus, for p-type contacts the Schottky barrier height is $E_g/2 + W_c - W_m$. Ohmic p-type contacts are obtained by using large work function metals, especially Pd, in combination with small band gap (i.e., large diameter) CNTs [4], so that the metal Fermi level falls near or below the CNT valence band edge.

Experimentally, it is prohibitively difficult to measure the actual CNT diameter in a statistically significant number of working devices. Nevertheless, one paper has reported the variation in $I_{\rm on}$ with diameter, for contacts made with several different metals [9]. Those authors note that their CNT diameter values are not entirely reliable, because they are inferred only indirectly, using a statistical analysis with a strong auxiliary assumption that variations in $I_{\rm on}$ for a given metal are due primarily to the CNT diameter. Even assuming that is correct, the statistics are only reliable for diameters in the middle of the range sampled. Nevertheless, in the absence of other data, that seminal work provides a natural starting point for comparison, and those data are included in Fig. 2.

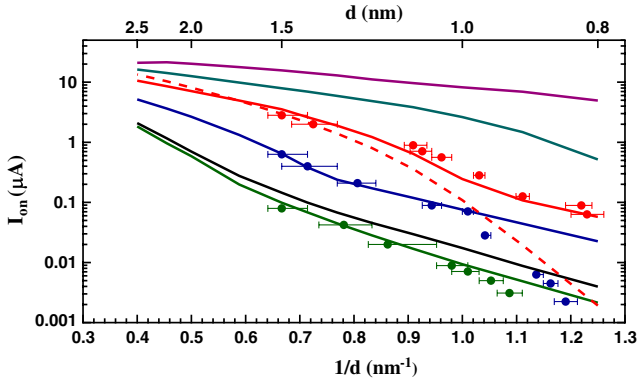

FIG. 2 (color online). On-state current $I_{\rm on}$ vs CNT inverse diameter (proportional to band gap), for different metal work functions from top to bottom: $\Delta W = W_m - W_c = 0.8, 0.5, 0.35, 0.23, 0.0, -0.1$ eV. The gate dielectric has thickness $t_{\rm ox} = 20$ nm, and $\epsilon = 3.9$ as for SiO_2. The symbols and error bars show experimental data from Ref. [9] for Pd, Ti, and Al metals, shown from top to bottom in red, cyan, and green circles, respectively. (We show only data for the range $1/d < 1.3$ nm^{-1} recommended in Ref. [9] as being relatively reliable.) The dashed line shows the current in the source-exhaustion limit, $I_{\rm se}$ from Eq. (3), for $\Delta W = 0.35$ eV, based on the self-consistent nonequilibrium carrier distribution.

We find a striking agreement between theory and experiment over 2 orders of magnitude in I_{on} in Fig. 2, if we take the work function for each metal as a fitting parameter. We actually use only the work function difference $\Delta W = W_m - W_c$ between metal and CNT midgap. In agreement with Ref. [9], we find that the work functions inferred in Fig. 2 vary by less than expected from literature values of the work functions. Most importantly, the fitted value $\Delta W = 0.35$ eV for Pd contacts is substantially smaller than the expected range $\Delta W \approx 0.9 \pm 0.2$ eV. This difference might simply reflect the fact that literature values of work function are for ultraclean surfaces in vacuum, while the actual devices have had prolonged exposure to air, and both metal and CNT may have picked up other impurities during the device processing, or more fundamental electronic-structure effects may play a role [18,19]. Figure 2 suggests the possibility of further improvements in device performance via work function engineering.

Ti and Al are well known to give Schottky contacts, and the behavior here is consistent with previous modeling. Narrow CNTs have larger band gaps, giving larger barrier heights. But the current decreases more slowly than for thermally activated transport, because it is dominated by tunneling. We note that in this regime, the detailed shape of the contacts as well as the work function can substantially influence the results [2,20].

The maximum possible current is expected to be governed by "source exhaustion" and "source starvation" [6–8]. This applies for ballistic devices with ideal Ohmic contacts, when the drain current V_d is large enough to reach saturation. In this limit, all the carriers in the CNT at the source end that are moving in the direction toward the channel are transmitted to the drain with probability 1. This carrier density depends on the self-consistent electrostatics of the CNT under the metal, with the actual nonequilibrium population of outgoing carriers. The corresponding current is

$$I_{se} = (4e/h)k_B T \ln[1 + \exp(E_{Fs}/k_B T)], \qquad (3)$$

where E_{Fs} is the Fermi level in the CNT under the source metal contact, relative to the valence band edge.

The calculated current I_{se} in this source-exhaustion limit is shown as a dashed line in Fig. 2 for the case of $\Delta W = 0.35$ eV (as for Pd contacts). The actual current can be less even for ballistic devices, because of additional electrostatic barriers [5]. We find that this is an important effect for very large work functions, but for $\Delta W = 0.35$ it is significant only for the largest diameters. In general, I_{se} gives a good semiquantitative description for the larger diameter CNTs.

For narrower tubes, the doping in the tube and I_{se} become exponentially small as the Fermi level falls deep in the band gap. The current, however, decreases more slowly, as it is dominated by tunneling to the metal, which represents a separate additional transport mechanism. From this perspective, it seems something of a coincidence that there is not a more striking change of slope in I_{on} vs $1/d$ when crossing between Schottky and Ohmic regimes, resulting from two quite different mechanisms giving a similar slope in I_{on} vs diameter.

Surprisingly, we find that $I_{on} > I_{se}$ for all devices in the diameter range of the experimental data. This indicates that tunneling is an important contribution even for nominally Ohmic devices. To understand this, in Fig. 3 we show the energy spectrum of the transmitted current. Here we focus on the case $\Delta W = 0.35$ eV and $d = 1.3$ nm, comparable to the best experimental devices. There is a large energy range where the source has states in the metal but not in the CNT. Carriers can tunnel from the metal to the channel via the evanescent modes of the CNT underneath the metal, as illustrated schematically in Fig. 1 (CNT region I), and through the external barrier in CNT region II. As the gate oxide gets thinner, the barrier becomes correspondingly thinner in Fig. 3(a), and so the tunneling current becomes increasingly important in Fig. 3(b). In contrast, the current contribution from propagating states is seen to be virtually independent of the gate oxide thickness.

Even for the 20 nm oxide, tunneling gives a 50% increase in I_{on} relative to the expected current I_{se} from propagating states. More advanced devices now use HfO_2, which has a larger dielectric constant than SiO_2, and which also allows fabrication of gate oxides as thin as 3 nm. Even thinner gate oxides can be made using Si oxynitride. We find that in the ballistic devices studied here, the dielectric constant has little impact, but the geometrical thickness is

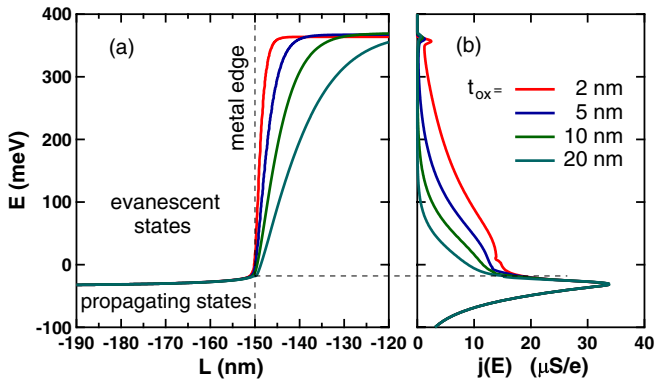

FIG. 3 (color online). Band bending and current distribution for a $d = 1.3$ nm CNT and metal $\Delta W = 0.35$ eV at overdrive $V_g - V_t = -0.5$ V and $V_d = -0.5$ V, for gate-oxide thicknesses $t_{ox} = 2$, 5, 10, 20 nm from top to bottom, respectively. (a) Valence band edge versus position. The zero of energy is the source Fermi level. The vertical dashed line shows position of the source metal edge at $L = -150$ nm. (b) Energy-resolved current density, Eq. (2), in the middle of the channel. Horizontal dashed line separates energies where CNT states are propagating versus evanescent in the source contact. The current contribution from the propagating states in (b) is $I_{se} \approx 1.3$ μA, nearly independent of t_{ox}. The total current is $I \approx 4.0$, 3.0, 2.4, and 2.0 μA for $t_{ox} = 2$, 5, 10, 20 nm, respectively.

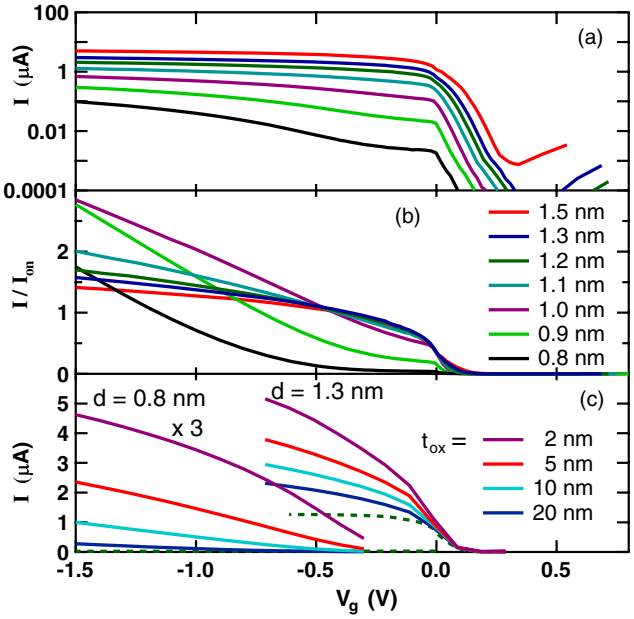

FIG. 4 (color online). (a) Transfer curves I vs V_g for different CNT diameters, for $V_d = -0.5$ V, $t_{ox} = 20$ nm, and $\Delta W = 0.35$ eV. (b) Same as (a) but on a linear scale, with each curve normalized to I_{on} at $V_g = V_t - 0.5$ V. ($I_{on} = 3.5$, 2.6, 1.9, 1.2, 0.64, 0.24, 0.11, and 0.057 μA for $d = 1.5$, 1.4, 1.3, 1.2, 1.1, 1.0, 0.9, and 0.8 nm, respectively.) (c) I vs V_g for CNT diameters $d = 0.8$ nm (left) and $d = 1.3$ nm (right), with $\Delta W = 0.35$ eV. Each diameter is shown for $t_{ox} = 2$, 5, 10, 20 nm from top to bottom. Note the multiplicative factor for $d = 0.8$ nm CNT in (c).

crucial. For the thinnest oxides, we find that the majority of the current comes from tunneling, even for the best devices. The quantitative values obtained here apply only to the specific geometry of Fig. 1, but the trends should apply very generally.

In Fig. 4 we show calculated transfer characteristics I-V_g for Pd contacts in devices with different CNT diameters. On a log scale, Fig. 4(a), the characteristics all appear rather similar. The most obvious difference is an overall reduction in current at smaller CNT diameters. We also note the appearance of ambipolar behavior with increasing diameter. (Even larger diameters would give higher current but lower on/off ratio, making such CNTs unsuitable for FETs.)

Figure 4(b) shows the same results plotted on a linear scale, after normalizing each curve by I_{on}. For the larger diameter CNTs, we see that the curves are still rather similar aside from the overall scaling by I_{on}. There is a relative sharp step in the current at threshold ($V_g \approx 0.11$ V). The current continues to rise with increasing V_g, and this nonsaturation is proportionally greater for the CNTs that are closer to the Ohmic-to-Schottky crossover. However, for the narrower CNTs the curves have qualitatively different shape, with no visible step in current, only a smooth increase.

In Fig. 4(c) we show calculated transfer characteristics for different oxide thicknesses, focusing on the case $\Delta W = 0.35$ eV and $d = 1.3$ nm as in Fig. 3. The dashed line shows the result for a 20 nm oxide, if we artificially suppress all tunneling. Results for other thicknesses are nearly the same when tunneling is suppressed, and all show the expected saturation corresponding to I_{se}. Such saturation is highly undesirable, since present technology is based on current increasing smoothly with V_g. In contrast, the full calculation shows no saturation with V_g, and increasingly high currents due to tunneling for thinner oxides and larger overdrives. Ultrathin oxides are considered desirable for many reasons, but here we find an entirely new reason: because they facilitate tunneling and hence forestall saturation with V_g. Figure 4(c) also shows results for a narrow CNT, $d = 0.8$ nm, corresponding to a Schottky contact. Then there is no step in current, because the current from propagating states is negligible compared to the tunneling current. There is only a smooth increase with V_g, with no very clear threshold for turn-on [21].

In summary, we have shown that the Ohmic-Schottky crossover in CNT-metal contact occurs with a smooth variation in on-state current, but a sharp change in the transfer characteristics. Typical high-performance devices operate close to the crossover, suggesting an opportunity for further performance improvements via work function engineering. These phenomena are directly relevant to other devices based on low-dimensional semiconductors, such as MoS_2 transistors [22], where contacts also play a limiting role in applications.

*Corresponding author.
tersoff@us.ibm.com

[1] R. Martel, V. Derycke, C. Lavoie, J. Appenzeller, K. K. Chan, J. Tersoff, and P. Avouris, Phys. Rev. Lett. **87**, 256805 (2001).
[2] S. Heinze, J. Tersoff, R. Martel, V. Derycke, J. Appenzeller, and P. Avouris, Phys. Rev. Lett. **89**, 106801 (2002).
[3] J. Appenzeller, J. Knoch, V. Derycke, R. Martel, S. Wind, and P. Avouris, Phys. Rev. Lett. **89**, 126801 (2002).
[4] A. Javey, J. Guo, Q. Wang, M. Lundstrom, and H. Dai, Nature (London) **424**, 654 (2003).
[5] A. W. Cummings and F. Léonard, Appl. Phys. Lett. **98**, 263503 (2011).
[6] J. Guo, S. Datta, M. Lundstrom, M. Brink, P. McEuen, A. Javey, H. Dai, H. Kim, and P. McIntyre, in *Proceedings of the Electron Devices Meeting, IEDM'02* (IEEE, New York, 2002), p. 711.
[7] M. V. Fischetti, L. Wang, B. Yu, C. Sachs, P. M. Asbeck, Y. Taur, and M. Rodwell, in *Proceedings of the Electron Devices Meeting, IEDM'07* (IEEE, New York, 2007), p. 109.
[8] L. Wei, D. J. Frank, L. Chang, and H.-S. P. Wong, IEEE Trans. Electron Devices **58**, 2456 (2011).
[9] Z. Chen, J. Appenzeller, J. Knoch, Y.-M. Lin, and P. Avouris, Nano Lett. **5**, 1497 (2005).

[10] A. W. Cummings and F. Léonard, ACS Nano **6**, 4494 (2012).
[11] S. Datta, *Quantum Transport Atom to Transistor* (Cambridge University Press, Cambridge, England, 2005).
[12] S. Jin, T.-W. Tang, and M. V. Fischetti, IEEE Trans. Electron Devices **55**, 727 (2008).
[13] See Supplemental Material at http://link.aps.org/supplemental/10.1103/PhysRevLett.111.236802 for a more complete description of the model.
[14] We focus on the case of a nearly ballistic channel, taking $v_F = 10^8$ cm/s, $\tau_{\text{scat}} v_F \gg L_{\text{ch}} = 300$ nm, and gate dielectric $\epsilon = 3.9$ as for SiO_2. To best match the electrostatics of the 10 nm back-gate geometry of Ref. [9] within our wrap-gate configuration, we take oxide thickness $t_{\text{ox}} = 20$ nm; see Ref. [15]. We checked that under the biasing conditions and device geometry used in the experiment, the acoustic and optical phonon scattering [16] with realistic coupling strengths do not significantly change the values of the on-state current. We use $\tau_M v_F = 100$ nm to account for the experimental transfer length [17] and long metal contacts $L_{\text{con}} = 600$ nm $\gg \tau_M v_F$. We include two subbands $i = 1, 2$. Temperature is 300 K throughout the Letter.
[15] R.-H. Yan, A. Ourmazd, and K. F. Lee, IEEE Trans. Electron Devices **39**, 1704 (1992).
[16] V. Perebeinos, J. Tersoff, and P. Avouris, Phys. Rev. Lett. **94**, 086802 (2005).
[17] A. D. Franklin and Z. Chen, Nat. Nanotechnol. **5**, 858 (2010).
[18] P. A. Khomyakov, G. Giovannetti, P. C. Rusu, G. Brocks, J. van den Brink, and P. J. Kelly, Phys. Rev. B **79**, 195425 (2009).
[19] G. Giovannetti, P. A. Khomyakov, G. Brocks, V. M. Karpan, J. van den Brink, and P. J. Kelly, Phys. Rev. Lett. **101**, 026803 (2008).
[20] S. Heinze, M. Radosavljevic, J. Tersoff, and P. Avouris, Phys. Rev. B **68**, 235418 (2003).
[21] Because there is no sharp threshold for turn-on in this regime, we define V_t as the value of V_g satisfying this condition: a tangent to the I-V_g curve taken at a 0.5 V below $V_g = V_t$ crosses $I = 0$ at $V_g = V_t$. This reduces to the conventional definition whenever a clear threshold exists.
[22] B. Radisavljevic, A. Radenovic, J. Brivio, V. Giacometti, and A. Kis, Nat. Nanotechnol. **6**, 147 (2011).

Supplemental Material: Schottky-to-Ohmic Crossover in Carbon Nanotube Transistor Contacts

V. Perebeinos, J. Tersoff, and W. Haensch
IBM T.J. Watson Research Center, Yorktown Heights, NY 10598, USA
(Dated: November 6, 2013)

DETAILS OF THE MODEL

To simulate the current flow in carbon nanotube field effect transistors (CNTFETs) we solve self-consistent Poisson equation for the electrostatics in the wrap-around gate geometry. For energies outside the bandgap, the distribution function $f_i^r(E,x)$ for right-moving carrier resolved by energy E and band index i obeys:

$$0 = -\frac{df_i^r(E,x)}{dx} + \frac{f_i^r(E,x) - f^0(E - E_F^M(x))}{v_i(E,x)\tau_M(E,x)} + \frac{f_i^r(E,x) - f^0(E - E_{loc}(x))}{v_i(E,x)\tau_{scat}(E,x)} \quad \text{(S1)}$$

where $v_i(E,x)$ is the band velocity and $f^0(x) = (\exp(x/k_BT) + 1)^{-1}$ is the Fermi-Dirac distribution, where $T = 300$ K throughout the paper. The second term describes an electrical coupling to the metal [*S1*], which provides a source of current into and out of the nanotube [*S2*]. Note, that for left-moving carriers $f_i^l(E,x)$, the sign of $v_i(E,x)$ in Eq. (S1) is opposite. The source and drain are ideal metals with respective Fermi-levels $E_F^M = 0$ and $E_F^M = W_s - W_d - eV_d$, where V_d is the applied source-drain bias, and W_s and W_d are the workfunctions of the source and drain electrodes. In Eq. (S1) we write $E_F^M(x)$ to indicate that the coupling (where nonzero) is to whichever contact is locally in contact. The third term allows thermalization of the carriers toward an equilibrium distribution within a relaxation-time approximation, with the local quasi-Fermi level $E_{loc}(x)$ found self-consistently [*S3*]. The timescales for carrier transfer between CNT and metal is determined by the CNT-metal coupling η_M, via $\tau_M(E,x) = \hbar\eta_M^{-1}(E,x)$. The scattering time $\tau_{scat}(E,x) = \hbar\eta_{scat}^{-1}(E,x)$ depends on the scattering rate η_{scat}.

For the propagating states, Eq. (S1) provides a complete formulation to find distribution function in the working CNT device. Where tunneling occurs, it is taken into account by appropriate boundary conditions at the classical turning points, see below. The electrostatic potential $\phi(x)$ defines a charge neutrality point (midgap for semiconducting tubes) $E_{NP}(x)$ according to

$$E_{NP}(x) = W_s - W_c - e\phi(x) \quad \text{(S2)}$$

where W_c is a (metallic) CNT workfunction, here taken to be 4.5 eV. We treat the CNT bandstructure within a rigid band approximation. So given the nanotube bandstructure, the local electronic structure is fully specified by an energy shift associated with the local potential: $E(k,x) = \varepsilon_k^i + E_{NP}(x)$, where k is the 1D wavevector along the CNT axis. Here we use $\varepsilon_k^i = \pm(\Delta_i^2 + \hbar^2 v_F^2 k^2)^{1/2}$ which has a single parameter $v_F \approx 10^8$ cm/s. A one dimensional wavevector along the CNT axis is k and the bandgap is $2\Delta_i$, where $\Delta_i = i \times 2\hbar v_F/3d$, where d is a CNT diameter and $i = 1, 2, 4, 5, ...$ (an integer which is not a multiple of 3).

We can express energy resolved current density j and total current I in the CNT as

$$j_i(E,x) = \frac{4e}{h}\left(f_i^r(E,x) - f_i^l(E,x)\right)$$
$$I(x) = \sum_i \int_{-\infty}^{\infty} j_i(E,x)dE \quad \text{(S3)}$$

which at any x is applicable for energies outside the local bandgap. For a given energy E, if x_1 and x_2 are the classical turning points where the band velocity vanishes, in the forbidden region between points x_1 and x_2 the tunneling current density is found from the boundary conditions imposing the current conservation:

$$f^l(E,x_1) = f^r(E,x_1)R_1 + T_1 f^0(E - E_F^M) + T_3 f^l(E,x_2)$$
$$f^r(E,x_2) = f^l(E,x_2)R_2 + T_2 f^0(E - E_F^M) + T_3 f^r(E,x_1) \quad \text{(S4)}$$

where E_F^M is the Fermi level inside the metal, reflection probabilities are $R_1 = 1 - T_1 - T_3$ and $R_2 = 1 - T_2 - T_3$. We approximate tunneling probabilities through the barrier $T_3 = P(x_1,x_2)$, to the metal from the left and from the right of the barrier T_1 and T_2, correspondingly, as:

$$T_1 = \int_{x_1}^{x_2} \alpha\kappa_M dx P(x_1,x), T_2 = \int_{x_1}^{x_2} \alpha\kappa_M dx P(x,x_2),$$
$$P(x',x'') = \exp\left[-\int_{x'}^{x''} dx\,(2\kappa(x) + \alpha\kappa_M)\right] \quad \text{(S5)}$$

where $\kappa(x) = (\Delta_i^2 - (E - E_{NP}(x))^2)^{1/2}/(\hbar v_F)$ and $\kappa_M = (\tau_M v_F)^{-1}$ are inverse tunneling and metal coupling lengths, correspondingly.

Eq. (S5) can be derived by assuming that the probability $P(x',x'')$ to find an electron at point x'', if $P(x',x') = 1$, is described by the differential equation $dP(x',x'') = -dx'' P(x',x'')(2\kappa(x'') + \alpha/(\tau_M v_F))$, where the first term gives carrier reduction due to the reflection and the second term due to the transfer to the metal.

We have tested approximation in Eq. (S5) against exact solutions for the tunneling probability from the transfer matrix method. For abrupt square well potentials, where the error is expected to be maximum, we find at most a factor of 2 discrepancy.

In general the value of α in Eq. (S5) depends on the energy of the incoming electron. It can be shown analytically that for the square well barrier, coupled to the metal by an imaginary energy $E \to E + i\eta_M$, and an incident carrier momentum $k_1 = (E - E_{NP})/(\hbar v_F)$ the value of α, in the limit of small η_M, is given by: $\alpha = 4\frac{\sqrt{k_1^2 - k_y^2}}{k_1 - \sqrt{k_y^2 - \kappa^2}}$, where $k_y = \Delta_i/(\hbar v_F)$.

For an arbitrary barrier shape, the potential outside the barrier depends on the distance away from the barrier. This leaves some ambiguities in the value of the effective α in Eq. (S5) that reproduces the exact tunneling probabilities $T_{i=1,2,3}$. In general k_1 outside the barrier is of the order of $2k_y$ and we are mainly interested in cases with small κ, so evanescent modes can propagate long distances under the barrier $\kappa \ll k_y$. Therefore, we approximate α by a constant $\alpha = 4\sqrt{3} \approx 7$.

SELF-CONSISTENT CNT DOPING

In the absence of tunneling, Eq. 3 of the main text:

$$I_{se} = \frac{4e}{h} k_B T \ln\left[1 + \exp\left(\frac{E_{Fs}}{k_B T}\right)\right] \qquad \text{(S6)}$$

provides a good estimate for the current. The CNT doping level E_{Fs} due to charge transfer from the metal is fully specified by the metal/CNT workfunction difference ΔW and CNT tube diameter. We use electrostatic distance $d_0 = 2.5$ Å to calculate metal-CNT capacitance $C_M = 2\pi\epsilon_0/\ln(1 + 2d_0/d)$ and charge carrier density

$$\rho = g \int_{-\infty}^{-\Delta_1} \frac{f^0(-E - E_{Fs} - \Delta_1)}{\pi\hbar v_F \sqrt{E^2 - \Delta_1^2}} E dE \qquad \text{(S7)}$$

which has to be found self-consistently with Eq. (S2), where $e\phi(x) = \rho/C_M$ under the metal. The results of the source exhaustion model [*S4*, *S6*] can be readily obtained by using degeneracy $g = 4$ in Eq. (S7), which is applicable in the low bias $|V_d| \ll E_{Fs}$ or in the diffusive limit, when carriers in opposite directions are at quasi-equilibrium. In ballistic channel and high bias $|V_d| \gg E_{Fs}$, the left and right moving carriers are described by Fermi distributions with different Fermi levels. Such that the source starvation effect takes place [*S5*], when hot carriers from the drain have occupancy of unity and don't contribute to the hole carrier density. This can be accounted for by using degeneracy $g = 2$ in Eq. (S7). We find that the effective g in Eq. (S7), i.e. the value that reproduces the self-consistent charge in the simulations, falls in the range $2 \le g \le 4$.

[S1] A. W. Cummings and F. Léonard, ACS Nano **6**, 4494 (2012).

[S2] S. Datta, Quantum Transport Atom to Transistor (Cambridge Univ. Press, 2005).

[S3] S. Jin, T.-W. Tang, M. V. Fischetti, IEEE Trans. on Elect. Dev. **55**, 727 (2008).

[S4] J. Guo, S. Datta, M. Lundstrom, M. Brink, P. McEuen, A. Javey, H. Dai, H. Kim, and M. McIntyre, IEDM Tech. Dig., **711** (2002).

[S5] M. V. Fischetti, L. Wang, B. Yu, C. Sachs, P. M. Asbeck, Y. Taur, and M. Rodwell, Proc. IEEE IEDM **109**, (2007).

[S6] L. Wei, D. J. Frank, L. Chang, H.-S. P. Wong, IEEE Trans. on Elect. Dev. **58**, 2456 (2011).